

Article

ZnO Particles Stabilized in Polymeric Matrix for Liquid-Phase Methanol Synthesis

Valentin Yu. Doluda ¹, Olga P. Tkachenko ² , Antonina A. Stepacheva ¹ , Alexander I. Sidorov ¹, Alexey V. Bykov ¹, Mikhail G. Sulman ^{1,*} and Yury Yu. Kosivtsov ¹ 

¹ Department of Biotechnology, Chemistry and Standardization, Tver State Technical University, 170026 Tver, Russia

² Laboratory of Developments and Study of Polyfunctional Catalysts, N.D. Zelinsky Institute of Organic Chemistry of Russian Academy of Science, 119991 Moscow, Russia

* Correspondence: sulmanmikhail@yandex.ru; Tel.: +7-(4822)-789348

Abstract: ZnO supported on hypercrosslinked polystyrene was developed for liquid-phase methanol synthesis. The synthesized catalyst was characterized using the low-temperature nitrogen physisorption, TEM, XPS, XAS, and CO DRIFT methods. The analysis showed that the catalyst has a high specific surface area (720 m²/g) and is characterized by the micro-mesoporous structure typical of the polymer used. The active phase is represented by ZnO species with a hexagonal wurtzite structure. ZnO-HPS showed high activity, selectivity, and stability in liquid-phase methanol synthesis in comparison with the industrial catalyst. The activity of the proposed catalyst was found to be 1.64 times higher than that of the conventional Cu/ZnO/Al₂O₃.

Keywords: methanol synthesis; ZnO catalyst; hypercrosslinked polystyrene



Citation: Doluda, V.Y.; Tkachenko, O.P.; Stepacheva, A.A.; Sidorov, A.I.; Bykov, A.V.; Sulman, M.G.; Kosivtsov, Y.Y. ZnO Particles Stabilized in Polymeric Matrix for Liquid-Phase Methanol Synthesis. *Catalysts* **2023**, *13*, 116. <https://doi.org/10.3390/catal13010116>

Academic Editor: Javier Ereña

Received: 21 November 2022

Revised: 26 December 2022

Accepted: 28 December 2022

Published: 4 January 2023



Copyright: © 2023 by the authors. Licensee MDPI, Basel, Switzerland. This article is an open access article distributed under the terms and conditions of the Creative Commons Attribution (CC BY) license (<https://creativecommons.org/licenses/by/4.0/>).

1. Introduction

Methanol is one of the key reactants in various fields of industry, i.e., pharmaceutical, cosmetic, perfumery, and fine chemistry. Methanol is also widely used for biodiesel production and can be applied as an alternative fossil fuel [1–4]. The production of methanol from biomass through gasification and subsequent CO hydrogenation is considered to be one of the prospective directions in green and sustainable chemistry [5–7].

Methanol can be produced in different ways: methane oxidation [8], the Christiansen process [9], two-step synthesis from methane through methyl-halide formation as an intermediate [10], and from synthesis gas [11–14]. The last process is currently used worldwide.

The synthesis of methanol from synthesis gas can be realized by either two- (gas phase) [15–18] or three-phase (liquid phase) processes [19,20]. Although gas-phase synthesis is widely studied, the high exothermic effect of the reaction requires the development of complex reactor systems [21]. Thus, liquid-phase methanol synthesis seems to be a promising method because of the simple reactor design, effective heat transfer, and lower process temperature [22–25]. Alcohols are the most often used solvents in liquid-phase methanol synthesis [26–28]. One of the main limitations of the liquid-phase process is considered to be the high catalyst deactivation rate [29,30]. However, this problem can be solved by the development of a stable and effective catalytic system.

In the industry, methanol synthesis from synthesis gas is carried out at the temperature of 240–270 °C and a pressure of 4.0–7.0 MPa. The typical catalyst used in this process is CuO/ZnO/Al₂O₃ [31–40]. The catalyst contains CuO (from 20 to 80%), ZnO (15–50%), and alumina (4–30%). Moreover, some additives can be used as promoters (i.e., MgO [41,42], ZrO₂ [43–45], Cr₂O₃ [43], and rare-earth metal oxides [41]). Cu particles are considered to be the main active components in methanol synthesis catalysts, while ZnO mainly provides the Cu dispersion [46,47]. However, some researchers showed that ZnO tends to be the active site in CO's hydrogenation into methanol [48,49]. Thus, in this work, the use of ZnO

particles supported on an inert polymeric matrix of hypercrosslinked polystyrene (HPS) in methanol synthesis is proposed. The use of polymers to stabilize the nanoparticles of transition metals and their oxides is an attractive possibility for the synthesis of efficient and stable catalysts, allowing modification of catalytic properties. The rigid polymers have a high surface area and both small and large mesopores, which are suitable for the formation of the active phase and substrate transport to the active sites [50–52].

2. Results and Discussion

2.1. Characterization of Catalyst Samples

Three catalyst samples—initial, treated with hydrogen, and after catalysis—were analyzed by low-temperature nitrogen physisorption. The obtained isotherms (IV type) of nitrogen adsorption for all studied samples correspond to those for micro-mesoporous materials (Figure 1a) [53]. The form of the hysteresis loop (H_4 type) indicates the presence of narrow slit-like pores for the studied samples (Figure 1b). Table 1 shows that during Zn incorporation into the polymer matrix a slight decrease in surface area is observed. Moreover, the decrease in the external surface area indicates the formation of ZnO particles in the polymer mesopores. For the catalyst treated with hydrogen at the reaction conditions, the surface area slightly decreases in comparison with the as-received catalyst. It indicates that no sufficient changes in the catalyst surface take place during the catalyst treatment. The decrease in surface area for the catalyst after the reaction can be connected with the absorption of reaction products into the pores of the polymer.

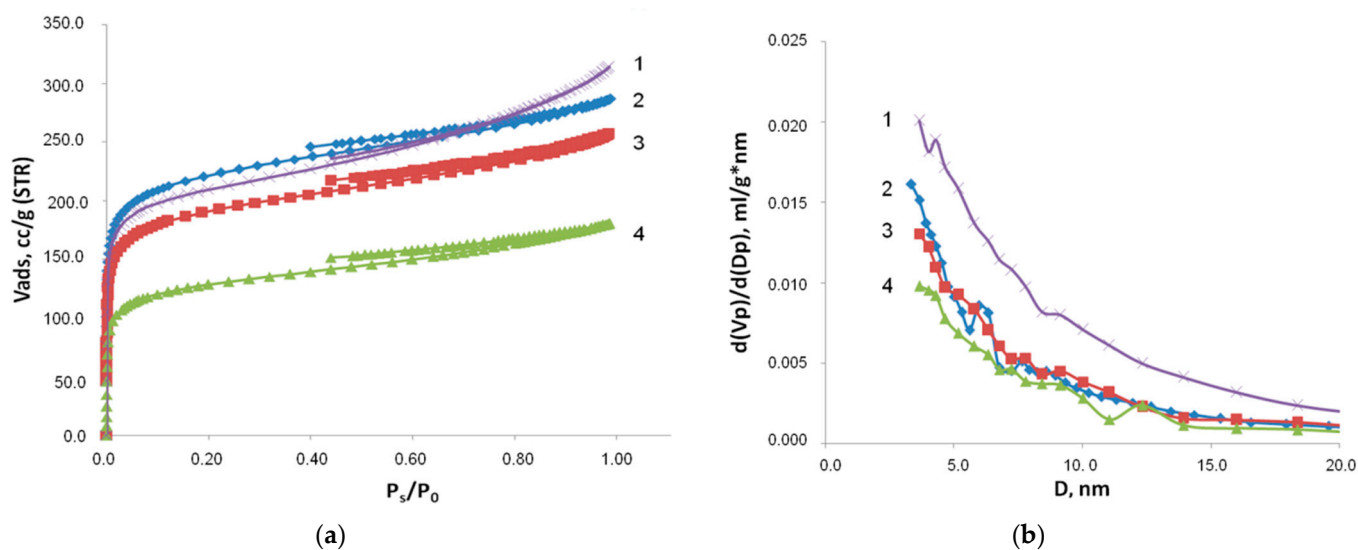


Figure 1. Results of BET studies: (a) adsorption isotherms; (b) pore size distribution for the catalyst samples: 1—HPS; 2—ZnO-HPS; 3—ZnO-HPS treated with hydrogen; 4—ZnO-HPS after catalysis.

Table 1. Catalyst surface area and pore volume.

Sample	V _{pores} , mL/g	S _{BET} , m ² /g	t-Plot Surface Area, m ² /g	D _{pores} , nm
HPS (MN-100)	0.57 ± 0.02	770 ± 1	External 135 ± 1 Micropore 635 ± 1	4–20
Initial ZnO-HPS	0.53 ± 0.02	723 ± 1	External 100 ± 1 Micropore 623 ± 1	4–20
Treated ZnO-HPS	0.53 ± 0.02	720 ± 1	External 98 ± 1 Micropore 622 ± 1	4–20
ZnO-HPS after catalysis	0.50 ± 0.02	693 ± 1	External 82 ± 1 Micropore 611 ± 1	4–20

TEM images of the three catalyst samples—initial, treated with hydrogen, and after catalysis, are presented in Figure 2. The study of the initial ZnO-HPS catalyst sample (Figure 2a) showed the presence of Zn-containing nanoparticles with a mean diameter of 8 nm. The treatment with hydrogen (Figure 2b) led to a slight increase in the particle size up to 8.5 nm. The catalyst sample after methanol synthesis (Figure 2c) also showed slight aggregation up to the size of 9.6 nm. A further increase in ZnO nanoparticle size was not observed.

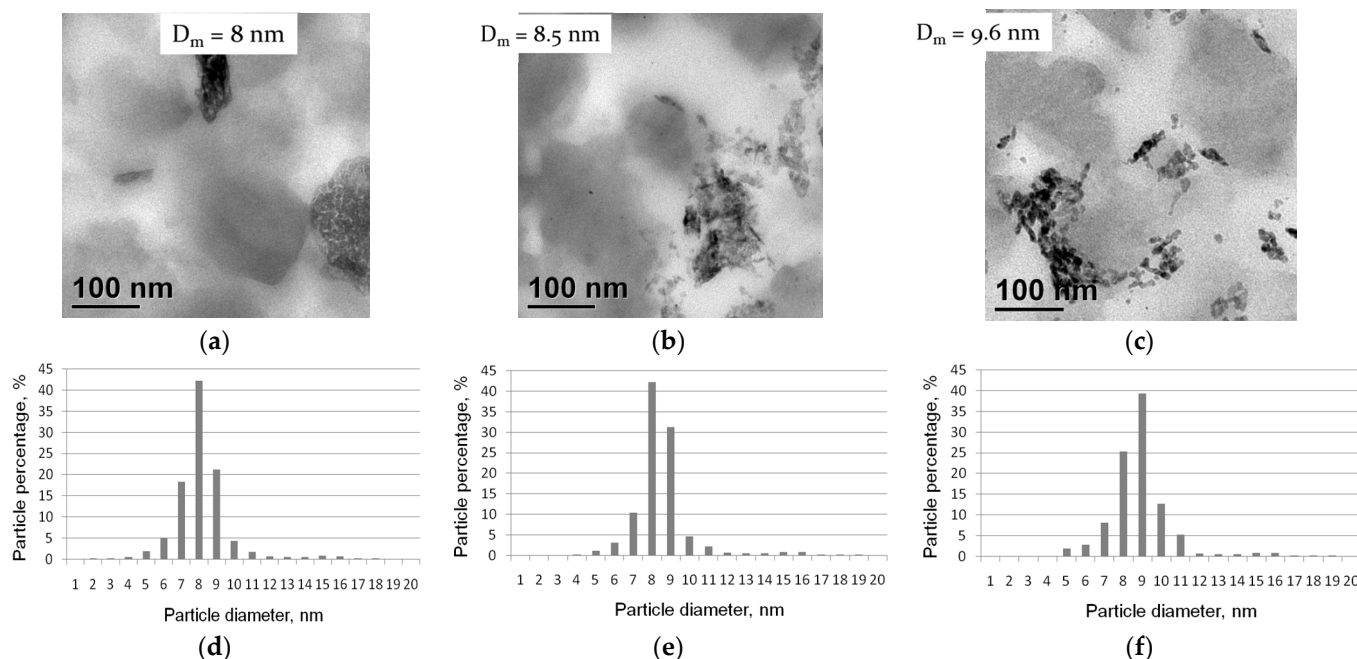


Figure 2. TEM images and particle size distribution histograms of the catalyst samples: (a,d) initial; (b,e) treated with hydrogen; (c,f) after catalysis.

The survey XPS spectra for the Zn-HPS-based catalyst samples show the presence of oxygen, carbon, zinc, and nitrogen on the polymer surface (Figures S1–S3). Chlorine was also observed as one of the contaminating agents. Moreover, chlorine ions can be absorbed by the polymer during its synthesis. From Table 2, it is seen that the treatment of the as-received catalyst with hydrogen at the reaction conditions leads to a negligible increase in Zn content on the catalyst surface from 1.2 up to 1.6 at. %, which can be attributed to the formation of additional ZnO clusters during the catalyst's saturation. However, such a difference is not significant and is within the permissible range of error. After the catalysis, a significant increase in the Zn surface content was observed (up to 3.6 at. %), which can be explained by the slight aggregation of the catalyst's active phase.

Table 2. Elemental composition of the catalyst surface.

Sample	Elemental Composition, at. %				
	C	O	N	Zn	Cl
Initial ZnO-HPS	85.7 ± 1.1	10.8 ± 0.2	1.8 ± 0.1	1.2 ± 0.1	0.5 ± 0.1
Treated ZnO-HPS	88.8 ± 1.1	7.5 ± 0.2	1.6 ± 0.1	1.6 ± 0.1	0.5 ± 0.1
ZnO-HPS after catalysis	81.8 ± 1.1	12.3 ± 0.2	1.7 ± 0.1	3.6 ± 0.1	0.6 ± 0.1

The deconvolution of the high-resolution XPS Zn 2p spectra (Figure 3a) results in one type of reactive species that can be attributed to ZnO [54–56]. Slight shifts in the binding energies for both Zn and O to higher values are attributed to the differential charging of the catalyst surface. The presented data are in accordance with those obtained in the XAS study.

The formation of ZnO crystals on the HPS surface was additionally confirmed by the XRD study (Figure S4) [57,58]. The analysis of XPS O 1s high-resolution spectra showed that the oxygen atoms present on the catalyst surface are attributed to ZnO species. However, for the as-synthesized catalyst sample, an additional peak at ~ 535.5 eV attributed to the adsorbed water was observed (Figure 3b).

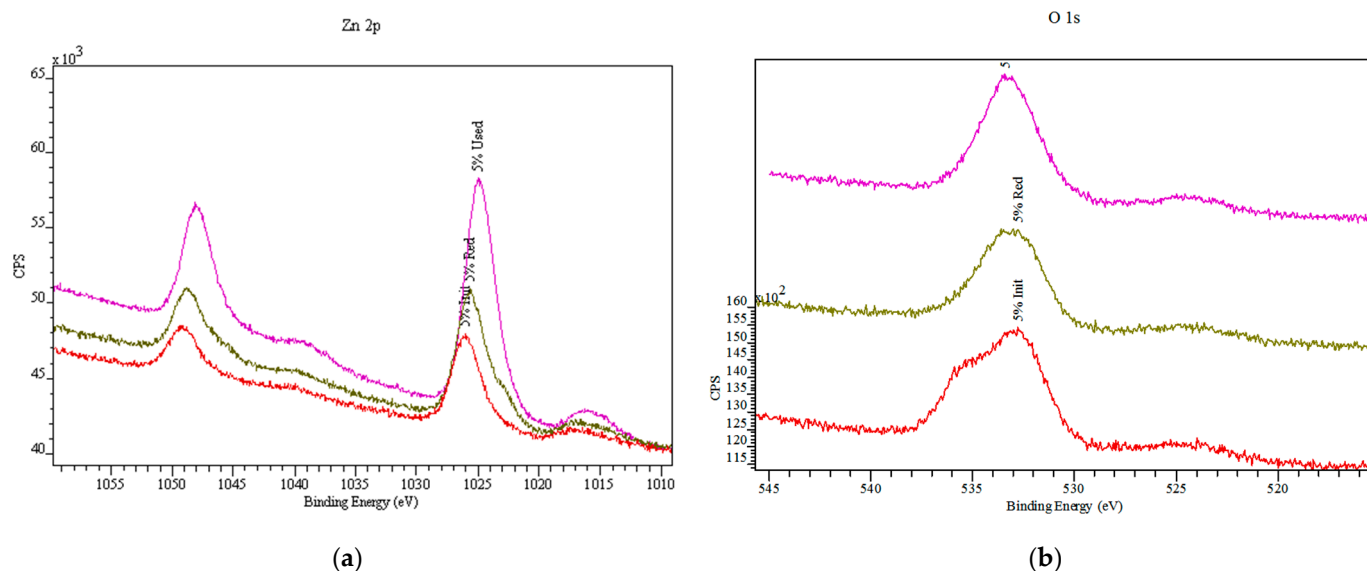


Figure 3. High-resolution XPS spectra: (a) Zn 2p detailed regions; (b) O 1s detailed regions: red line—as-synthesized catalyst; yellow line—catalyst treated with hydrogen; violet line—catalyst after testing.

To estimate the structure of the catalytically active sites of the ZnO-HPS catalyst, the three samples—ZnO-HPS initial (as received), treated with H_2 , and after catalysis—were studied by XAS analysis. Figure 4 shows the Zn K XANES of these zinc samples with the ZnO reference compound. The position of the Zn K-edge in all spectra of the ZnO-HPS catalysts is similar to that in the spectrum of the ZnO reference. This means that Zn in all catalyst samples exists in the Zn^{2+} electronic state, as was expected.

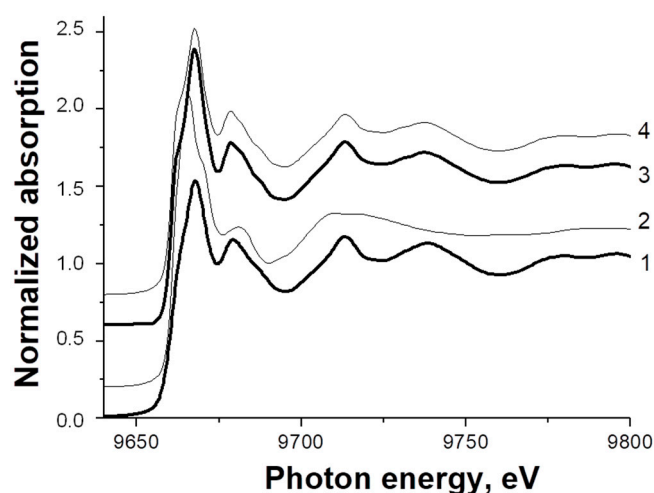


Figure 4. Zn XANES of the Zn samples: 1—ZnO reference; 2—ZnO-HPS initial; 3—ZnO-HPS treated; 4—ZnO-HPS after the catalysis.

Furthermore, one can deduce by analyzing the intensity of the white line that the Zn species in the initial sample is, on average, surrounded by more electron-acceptor neighbors, whereas both treated samples and samples after the reaction demonstrate more

electron-donor neighbors, which can be attributed to dynamic morphology changes in the catalyst structure, mainly due to the saturation of ZnO clusters with hydrogen and partial ZnO reduction, thus leading to changes in oxidation potential and surface energy [59].

The Fourier transformation of EXAFS oscillations for the three ZnO-HPS samples and references is presented in Figure 5. There are two narrow peaks in the spectrum of the ZnO reference. The first peak corresponds to the first and second coordination shells containing, respectively, one and three oxygen atoms at 1.79 and 2.04 Å real distances from the central Zn atom. The second peak corresponds to the third and fourth coordination shells containing, respectively, six and six zinc atoms at 3.21 and 3.25 Å real distances from the central Zn atom [60].

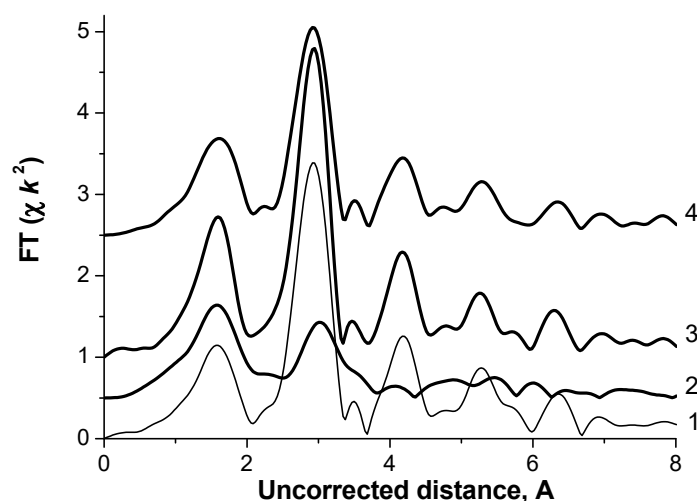


Figure 5. FT of Zn K EXAFS spectra of the Zn samples: 1—ZnO reference; 2—ZnO-HPS initial; 3—ZnO-HPS treated; 4—ZnO-HPS after catalysis.

The FT EXAFS spectra of both ZnO-HPS treated samples and samples after catalysis are similar to those of the ZnO reference, whereas the FT EXAFS spectra of the ZnO-HPS initial sample show second peaks at a higher uncorrected distance. In addition, the intensity of the second peak differs in the FT EXAFS spectra of all three ZnO-HPS samples. The first and second peaks of the Zn FT EXAFS spectra were fitted in both *r*- and *k*-spaces with a two-shell model—oxygen and zinc shells around the central absorbing Zn atom (Figures S5–S7). The results of the model fit are presented in Table 3.

Table 3. Parameters of the best model fit of Zn K EXAFS spectra of ZnO-HPS samples.

Sample	Path	R, Å	CN	$\sigma \times 10^{-3}, \text{Å}^{-2}$	$\Delta E, \text{eV}$
Initial	Zn–O	2.04 ± 0.01	3.3 ± 0.2	8.2 ± 1	11.6 ± 0.9
	Zn–Zn	3.26 ± 0.01	4.7 ± 0.6	9.8 ± 1	23.1 ± 1.3
Treated	Zn–O	2.00 ± 0.02	3.2 ± 0.6	5.2 ± 2.3	13.9 ± 3.4
	Zn–Zn	3.22 ± 0.05	11.3 ± 1.1	6.1 ± 0.7	7.5 ± 0.8
After catalysis	Zn–O	2.02 ± 0.02	3.4 ± 0.7	7.6 ± 2.0	15.0 ± 3.2
	Zn–Zn	3.22 ± 0.01	10.2 ± 1.1	7.8 ± 0.8	6.8 ± 1.0

It is seen that the first shell contains three O atoms at a real distance of 2.04 Å and the second shell contains five Zn atoms at a real distance of 3.26 Å in the initial sample. The first shell contains three O atoms at a real distance of 2.00–2.02 Å in both treated samples and samples after the reaction. The second shell contains 10–11 Zn atoms at a real distance of 3.22 Å in these samples. The increase in Zn atom content in the structure of the ZnO active site can be connected with a partial reduction in ZnO species. As was proposed by [61], the decrease in oxygen content in zinc oxide clusters leads to a decrease in the interface energy, thereby leading to the enhancement of the catalyst–substrate interaction and an increase

in catalytic activity. Thus, the treatment of the initial catalyst with hydrogen allows an increase in the catalytic performance. The insufficient changes in Zn atom content in the case of the used catalyst indicate that the catalyst maintains its morphology and thereby its activity. Thus, it can be proposed that the active site of the synthesized catalyst has a Zn–O–Zn cluster structure, where Zn atoms are dissolved in ZnO. Moreover, the saturation of catalysts with hydrogen leads to the formation of larger clusters (in comparison with the as-received catalyst) with a plane form.

Figure 6 represents the IR spectra of CO diffusion reflection registered for the three ZnO-HPS catalysts: initial, treated with hydrogen, and after the catalysis.

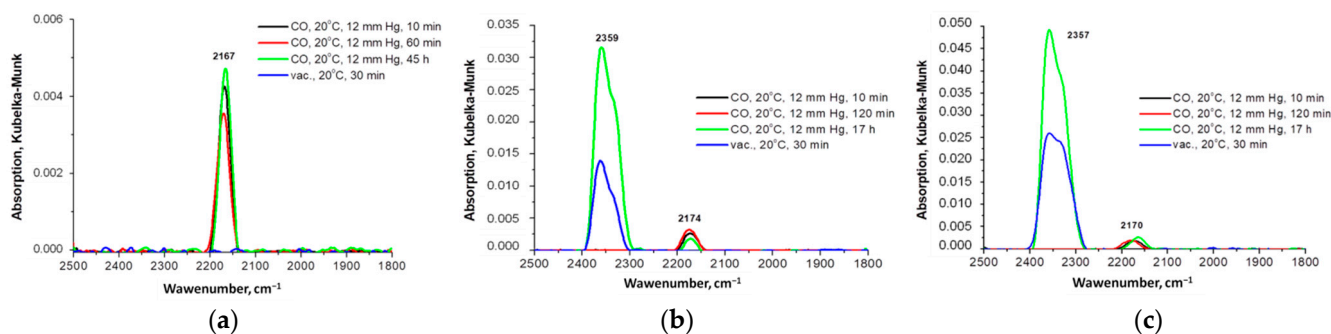


Figure 6. CO DRIFT spectra for the ZnO-HPS catalyst samples: (a) initial, (b) treated with hydrogen, (c) after catalysis.

After CO adsorption at room temperature, one low-intensity absorption band at 2167 cm^{-1} is observed in the spectra of the initial sample (Figure 6a). This band corresponds to the valent vibrations of the CO molecule adsorbed on Zn^{2+} in the linear form. In the spectra of the catalyst sample treated with hydrogen, an absorption band at 2174 cm^{-1} attributed to the valent vibrations of CO adsorbed on Zn^{2+} in linear form is observed (Figure 6b). After holding the sample at room temperature for 17 h, the intensity of the absorption band at 2174 cm^{-1} decreased, while the band at 2359 cm^{-1} was attributed to the appearance of adsorbed CO_2 molecules. In the IR spectra of the catalyst sample after catalysis (Figure 6c), the adsorption bands at 2170 cm^{-1} and 2357 cm^{-1} attributed to the vibrations of CO and CO_2 adsorbed on Zn^{2+} , respectively, are observed.

2.2. Catalytic Performance Study

The synthesized catalyst testing in methanol synthesis showed that the methanol yield reached up to $513\text{ g(MeOH)/(kg(cat)\cdot h)}$, compared to $312\text{ g(MeOH)/(kg(cat)\cdot h)}$ in the case of the conventional $\text{Cu/ZnO/Al}_2\text{O}_3$ catalyst reported in [24], as well as to the MEGAMAX[®] 700 catalyst, which afforded a methanol yield reaching up to $118\text{ g(MeOH)/(kg(cat)\cdot h)}$. The formation of methane as the main byproduct for the synthesized catalyst reached up to $86\text{ mg(CH}_4\text{)/(kg(cat)\cdot h)}$, while, for MEGAMAX[®] 700, methane formation was over $350\text{ mg(CH}_4\text{)/(kg(cat)\cdot h)}$. Moreover, the developed catalyst showed high activity at a lower temperature ($170\text{ }^\circ\text{C}$) compared to a commonly applied temperature of $250\text{--}270\text{ }^\circ\text{C}$. Figure 7 shows that the ZnO-HPS catalyst maintains and even slightly increases its activity and selectivity up to 100 h, while, for the industrial catalyst, there was observed a slight decrease in catalytic performance at long-term operation (see Table 4).

Table 4. Catalyst testing results.

Sample	CO Conversion, mol.%	MeOH Selectivity, mol.%	Selectivity after 100 h, mol.%
ZnO-HPS	67.2	99.8	99.8
MEGAMAX [®] 700	30.4	97.5	95.3
$\text{Cu/ZnO/Al}_2\text{O}_3$ [24]	44.5	99.4	97.8

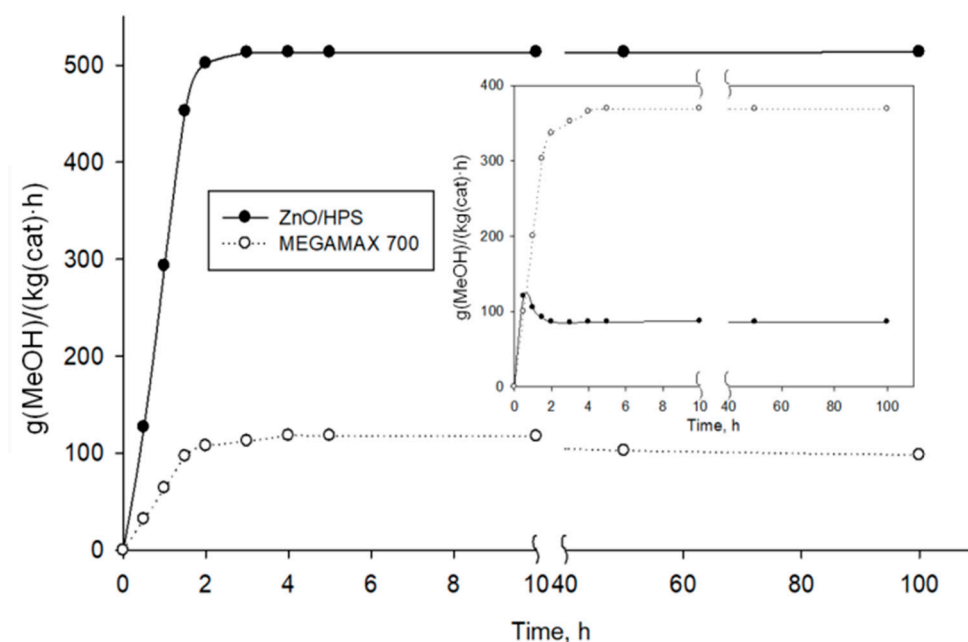


Figure 7. Methanol and methane formation curve in the presence of ZnO-containing catalysts.

3. Materials and Methods

3.1. Materials

Hypercrosslinked polystyrene (HPS) Macronet MN100 (functional groups—tert-amino groups, weak base capacity 0.5 mol/L, moisture 55–62%, swell factor max $\pm 5\%$, specific gravity 1.04 g/mL, specific surface area 790 m²/g) was purchased from Purolite Int. (Llantrisant, U.K.) and used as received as a catalyst support. Zinc acetate (chemical grade, Sigma Aldrich, St. Louis, MO, USA) was used as a ZnO precursor. Tetrahydrofuran (chemical grade, Sigma Aldrich, USA) and methanol (chemical grade, Sigma Aldrich, St. Louis, MO, USA) were used as received for catalyst preparation. Isopropyl alcohol (IPA) (chemical grade, Kupavna Reactive, Moscow, Russia) and n-dodecane (chemical grade, Kupavna Reactive, Moscow, Russia) were used as solvents in methanol synthesis. H₂ (99.9%, GasProduct, Tver, Russia), N₂ (99.9%, GasProduct, Tver, Russia), CO (99.9%, GasProduct, Tver, Russia), and CO₂ (99.9%, GasProduct, Tver, Russia) were used for methanol synthesis.

3.2. ZnO Catalyst Synthesis

The catalyst was prepared by the wet impregnation of HPS with 0.4225 g of Zn(Ac)₂ in a solution containing 5.0 mL of tetrahydrofuran, 1.0 mL of methanol, and 3.0 mL of distilled water for 3.0 g of MN-100. The suspension was continuously stirred for 10 min to allow the adsorption of the solution by the polymer granules. Then, the resulting granules were dried at 75 °C for 1 h. The catalyst was washed with water at pH 6.4–7.0 and dried at 75 °C for 3 h and then heated up to 250 °C for 5 h under a nitrogen flow to form ZnO. Zn content was found to be 5.0 wt. % by X-ray fluorescent elemental analysis using Zeiss Jena VRA-30 (Zeiss, Jena, Germany).

3.3. Catalyst Characterization

The specific surface area, porosity, and pore size distribution of the catalyst samples (initial, after saturation with hydrogen, and after catalysis) were determined by nitrogen low-temperature adsorption using a Beckman Coulter SA 3100 (Coulter Corporation, Brea, CA, USA) analyzer. Before the analysis, the samples were outgassed in a Beckmann Coulter SA-PREP (Coulter Corporation, Brea, CA, USA) apparatus for sample preparation at 120 °C in a vacuum for 1 h. To estimate the specific surface area and total pore volume, the t-plot and Brunauer–Emmett–Teller models were used. Pore size distribution was evaluated using the Harkins–Jure equation.

The transmission electron microscopy (TEM) study of the catalyst samples (see before) was performed using a JEOL JEM1010 scanning transmission electron microscope (JEOL Ltd., Tokyo, Japan) operating at 80 kV. The polymer-based samples were embedded in an epoxy resin and microtomed in cross-sections. Images of the resulting thin sections (ca. 100 nm thick) were collected with a Gatan digital camera (Gatan Inc., Pleasanton, CA, USA) and analyzed with the Adobe Photoshop software package and the Scion Image Processing Toolkit (Scion Corporation, Chicago, IL, USA).

X-ray photoelectron spectroscopy (XPS) analysis of ZnO-HPS was performed using an ES-2403 spectrometer (Institute for Analytical Instrumentation RAS, St. Petersburg, Russia) modified with an analyzer, the PHOIBOS 100 produced by SPECS GmbH (Berlin, Germany), equipped with a MgK α /AlK α XR-50 X-ray radiation source. The spectra were acquired at an X-ray power of 200 W and an energy step of 0.1 eV. Before the analysis, the samples were allowed to outgas for 180 min. The data analysis was performed using CasaXPS (Casa Software Ltd, Teignmouth, U.K.).

X-ray absorption spectroscopy measurements were carried out on the BM23 station of The European Synchrotron Radiation Facility (Grenoble, France). Zn K (9659 eV) X-ray absorption spectra were recorded in the transmission mode using a Si (111) double-crystal monochromator. The samples, pressed into self-supporting wafers, were measured at 30 K. The spectrum of a metal foil was recorded simultaneously between the second and a third ionization chamber for energy calibration purposes. Special care was taken to avoid ambient atmosphere contamination. For sample preparation, the optimum weight to maximize the signal-to-noise ratio was pressed into a 13 mm diameter pellet in a glove bag (a dried He atmosphere) and completely wrapped in polyimide (Kapton, DuPont, Wilmington, DE, USA) adhesive tape. The analysis of the EXAFS spectra was performed with the software VIPER (Oriux, Houston, TX, USA) for Windows. The required scattering amplitudes and phase shifts were calculated by the ab initio FEFF8.10 code [62,63] for ZnO. At least duplicate spectra were recorded to ensure data reproducibility. The fitting was done in the k- and r-spaces. The shell radius r , coordination number N , Debye–Waller factor σ^2 , and adjustable “muffin-tin zero” ΔE were determined as fitting parameters. The errors of the fitting parameters were found by decomposition of the statistical χ^2 function near its minimum, taking into account maximal pair correlations.

IR spectra of CO diffusion reflection were registered using an IR spectrometer, the NICOLET “Protege” 460 (Thermo Fisher Scientific, Waltham, MA, USA). Before the analysis, the catalyst samples were pretreated in a vacuum for 3 h at room temperature. Carbon monoxide was used as a test molecule. The adsorption of CO was performed at room temperature at a pressure of 12 mm Hg. CO desorption was carried out in a vacuum. Spectra were registered in the range of 6000–400 cm^{-1} with a step of 4 cm^{-1} .

3.4. Catalytic Performance Study

The catalyst testing was performed in the flow-mode reactor reported in [64]. The catalyst was preliminarily treated at the reaction temperature (170 °C) in 30 mL/min hydrogen flow before the reaction to saturate the catalyst’s active sites with hydrogen. As is known [65], Zn oxide cannot be reduced to the metal state at this temperature, so we expected the presence of ZnO particles in the treated catalyst. A typical experiment was carried out as follows: 0.5 g of the catalyst in 45.0 mL of a solvent consisting of 15.0 mL of isopropyl alcohol (IPA) and 30.0 mL of dodecane was loaded in the reactor, which was equipped with a propeller mixer (stirring rate 250 rpm). Then, the hydrogen pressure was set at 3.0 MPa with a flow of 45 mL/min and the mixture was heated up to 170 °C. After the catalyst’s saturation for 1 h, hydrogen was substituted for synthesis gas composed of 79.38% H₂, 0.12% N₂, 20.49% CO, and 0.01% CO₂, and the stirring rate was increased up to 750 rpm. The synthesis gas pressure was set at 2.0 MPa with a gas feeding rate of 270 mL/min. The reaction temperature was 170 °C. Under the same conditions, we also tested an industrial Cu-Zn-containing catalyst MEGAMAX[®] 700 (Süd-Chemie AG, Moosburg an der Isar, Germany). The outgoing steam-gas flow was directed into the

chromatographic system of an online analysis tool (Kristallux 4000, Meta-Chrom, Yoshkar-Ola, Russia) along the heated line through the return pressure valve and removed from the system through a flow meter.

4. Conclusions

A ZnO-HPS catalyst was synthesized and applied for liquid-phase methanol synthesis. The catalyst has a high specific surface area, allowing the transfer of the reactants and products to the active sites. The characterization of the synthesized catalyst showed that the active phase of ZnO-HPS is represented by ZnO species with a mean particle diameter of approximately 8 nm, formed on the surface of the polymer. The ZnO nanoparticles have a hexagonal wurtzite structure. Moreover, the catalyst structure practically does not change during the reaction. The synthesized ZnO embedded into a polymeric matrix of HPS was found to be an active, selective, and stable catalyst for liquid-phase methanol synthesis, allowing a decrease in the reaction temperature from the conventional 250–270 °C to 170 °C.

Supplementary Materials: The following supporting information can be downloaded at: <https://www.mdpi.com/article/10.3390/catal13010116/s1>, Figure S1: The survey XPS spectra for the initial Zn-HPS; Figure S2: The survey XPS spectra for the Zn-HPS treated with hydrogen; Figure S3: The survey XPS spectra for the Zn-HPS after catalysis; Figure S4: XRD pattern for the Zn-HPS; Figure S5: Model fits of Zn K EXAFS of ZnO-HPS initial samples in k-space (a) and r-space (b); Figure S6: Model fits of Zn K EXAFS of ZnO-HPS treated samples in k-space (a) and r-space (b); Figure S7: Model fits of Zn K EXAFS spectrum of ZnO-HPS after catalysis sample in k-space (a) and r-space (b).

Author Contributions: Conceptualization, V.Y.D., A.I.S., M.G.S.; methodology, A.I.S.; investigation, O.P.T., A.V.B., V.Y.D., A.A.S.; writing—original draft preparation, A.A.S.; writing—review and editing, A.A.S.; project administration, Y.Y.K. All authors have read and agreed to the published version of the manuscript.

Funding: The financial support for the work was provided by the Russian Science Foundation (grant No 20-69-47084).

Data Availability Statement: Not applicable.

Conflicts of Interest: The authors declare no conflict of interest.

References

1. Farsi, M.; Jahanmiri, A. Application of water vapor-permselective alumina–silica composite membrane in methanol synthesis process to enhance CO₂ hydrogenation and catalyst life time. *J. Ind. Eng. Chem.* **2012**, *18*, 1088–1095. [[CrossRef](#)]
2. Olah, G.A. Towards Oil Independence Through Renewable Methanol Chemistry. *Angew. Chem. Int. Ed.* **2012**, *52*, 104–107. [[CrossRef](#)] [[PubMed](#)]
3. Choudhury, J. New Strategies for CO₂-to-Methanol Conversion. *ChemCatChem* **2012**, *4*, 609–611. [[CrossRef](#)]
4. Din, I.U.; Shaharun, M.S.; Alotaibi, M.A.; Alharthi, A.I.; Naeem, A. Recent developments on heterogeneous catalytic CO₂ reduction to methanol. *J. CO₂ Util.* **2019**, *34*, 20–33. [[CrossRef](#)]
5. Gautam, P.; Upadhyay, S.N.; Dubey, S.K. Bio-methanol as a renewable fuel from waste biomass: Current trends and future perspective. *Fuel* **2020**, *273*, 117783. [[CrossRef](#)]
6. Detchusananard, T.; Prasertcharoensuk, P.; Patcharavorachot, Y.; Maréchal, F.; Arpornwichanop, A. Exergy and exergoeconomic assessment of sustainable light olefins production from an integrated methanol synthesis and methanol-to-olefins system. *J. Clean. Prod.* **2022**, *347*, 131209. [[CrossRef](#)]
7. Im-orb, K.; Arpornwichanop, A. Process and sustainability analyses of the integrated biomass pyrolysis, gasification, and methanol synthesis process for methanol production. *Energy* **2020**, *193*, 116788. [[CrossRef](#)]
8. Olah, G.A.; Prakash, G.K.S. Efficient and Selective Conversion of Carbon Dioxide to Methanol, Dimethyl Ether and Derived Products. Patent EP1871731B1, 26 December 2012.
9. Christiansen, J.A. Method of Producing Methyl Alcohol from Alkyl Formate. U.S. Patent No 1,302-011, 29 April 1919.
10. Olah, G.A.; Gupta, B.; Farina, M. Selective monohalogenation of methane over supported acid or platinum metal catalysts and hydrolysis of methyl halides over gamma-alumina-supported metal oxide/hydroxide catalysts. A feasible path for the oxidative conversion of methane into methyl alcohol/dimethyl ether. *J. Am. Chem. Soc.* **1985**, *107*, 7097–7105.
11. Deutschmann, O.; Knozinger, H.; Kochloefl, K.; Turek, T. *Heterogeneous Catalysis and Solid Catalysts*; Wiley-VCH Verlag GmbH & Co. KGaA: Weinheim, Germany, 2009; pp. 82–93.

12. Li, Y.; Sorribes, I.; Yan, T.; Junge, K.; Beller, M. Selective methylation of amines with carbon dioxide and H₂. *Angew. Chem.* **2013**, *52*, 12156–12160. [[CrossRef](#)]
13. Li, C.; Yuan, X.; Fujimoto, K. Development of highly stable catalyst for methanol synthesis from carbon dioxide. *Appl. Catal. A Gen.* **2014**, *469*, 306–311. [[CrossRef](#)]
14. Karelavic, A.; Ruiz, P. The role of copper particle size in low pressure methanol synthesis via CO₂ hydrogenation over Cu/ZnO catalysts. *Catal. Sci. Technol.* **2015**, *5*, 869–881. [[CrossRef](#)]
15. Pinto, A.; Rogerson, P.L. Impact of high fuel cost on plant design. *Chem. Eng. Prog.* **1977**, *73*, 95–100.
16. Haid, J.; Koss, U. Lurgi's Mega-Methanol technology opens the door for a new era in down-stream applications. *Stud. Surf. Sci. Catal.* **2001**, *136*, 399–404.
17. Takase, I.; Niwa, K. Mitsubishi (MGC/MHI) methanol process CEER. *Chem. Econ. Eng. Rev.* **1985**, *17*, 24–30.
18. Fiedler, E.; Grossmann, G.; Kersebohm, D.B.; Weiss, G.; Witte, C. Methanol. In *Ullmann's Encyclopedia of Industrial Chemistry Release*, 6th ed.; Wiley-VCH, Verlag GmbH & Co. KGaA: Weinheim, Germany, 2003; pp. 1–23.
19. Wang, J.; Anthony, R.G.; Akgerman, A. Mathematical simulations of the performance of trickle bed and slurry reactors for methanol synthesis. *Comput. Chem. Eng.* **2005**, *29*, 2474–2484. [[CrossRef](#)]
20. Heydorn, E.C.; Diamond, B.W.; Lilly, R.D. *Commercial-Scale Demonstration of the Liquid Phase Methanol (LPMEOH) Process: Final Report*; Air Products Liquid Phase Conversion Company for the US DOE National Energy Technology Laboratory: Allentown, PA, USA, 2003.
21. Nassirpour, M.; Khademi, M.H. Evaluation of different cooling technologies for industrial methanol synthesis reactor in terms of energy efficiency and methanol yield: An economic-optimization. *J. Taiwan Inst. Chem. Eng.* **2020**, *113*, 302–314. [[CrossRef](#)]
22. Van der Laan, G.P.; Beenackers, A.A.C.M.; Ding, B.; Strikwerda, J.C. Liquid-phase methanol synthesis in apolar (squalane) and polar (tetraethylene glycol dimethylether) solvents. *Catal. Today* **1999**, *48*, 93–100. [[CrossRef](#)]
23. Schimpf, S.; Rittermeier, A.; Zhang, X.; Li, Z.-A.; Spasova, M.; van den Berg, M.W.E.; Farle, M.; Wang, Y.; Fischer, R.A.; Muhler, M. Stearate-Based Cu Colloids in Methanol Synthesis: Structural Changes Driven by Strong Metal-Support Interactions. *ChemCatChem* **2010**, *2*, 214–222. [[CrossRef](#)]
24. Zhang, X.; Zhong, L.; Guo, Q.; Fan, H.; Zheng, H.; Xie, K. Influence of the calcination on the activity and stability of the Cu/ZnO/Al₂O₃ catalyst in liquid phase methanol synthesis. *Fuel* **2010**, *89*, 1348–1352. [[CrossRef](#)]
25. Mabuse, H.; Hagihara, K.; Watanabe, T.; Saito, M. Liquid phase methanol synthesis catalyst. *Energy Convers. Manag.* **1997**, *38*, S437–S442. [[CrossRef](#)]
26. Meesattham, S.; Kim-Lohsoontorn, P. Low-temperature alcohol-assisted methanol synthesis from CO₂ and H₂: The effect of alcohol type. *Int. J. Hydrog. Energy* **2022**, *47*, 22691–22703. [[CrossRef](#)]
27. Kriprasertkul, W.; Witoon, T.; Kim-Lohsoontorn, P. Dimethyl ether (DME) synthesis from CO₂ and H₂ through ethanol-assisted methanol synthesis and methanol dehydration. *Int. J. Hydrog. Energy* **2022**, *47*, 33338–33351. [[CrossRef](#)]
28. Boonamnuay, T.; Laosiripojana, N.; Assabumrungrat, S.; Kim-Lohsoontorn, P. Effect 3A and 5A molecular sieve on alcohol-assisted methanol synthesis from CO₂ and H₂ over Cu/ZnO catalyst. *Int. J. Hydrog. Energy* **2021**, *46*, 30948–30958. [[CrossRef](#)]
29. Kung, H.H. Deactivation of methanol synthesis catalysts—A review. *Catal. Today* **1992**, *11*, 443–453. [[CrossRef](#)]
30. Lee, S. *Methanol Synthesis Technology*; CRC Press: Boca Raton, FL, USA, 1990.
31. Klier, K.; Chatikavanij, V.; Herman, R.G.; Simmons, G.W. Catalytic synthesis of methanol from CO/H₂: IV. The effects of carbon dioxide. *J. Catal.* **1982**, *74*, 343–360. [[CrossRef](#)]
32. Cazelles, R.; Drone, J.; Fajula, F.; Ersen, O.; Moldovan, S.; Galarneau, A. Reduction of CO₂ to methanol by a polyenzymatic system encapsulated in phospholipids-silica nanocapsules. *New J. Chem.* **2013**, *37*, 3721–3730. [[CrossRef](#)]
33. Frei, E.; Schaadt, A.; Ludwig, T.; Hillebrecht, H.; Krossing, I. The Influence of the Precipitation/Ageing Temperature on a Cu/ZnO/ZrO₂ Catalyst for Methanol Synthesis from H₂ and CO₂. *ChemCatChem* **2014**, *6*, 1721–1730. [[CrossRef](#)]
34. Gao, P.; Li, F.; Zhan, H.; Zhao, N.; Xiao, F.; Wei, W.; Zhong, L.; Sun, Y. Fluorine-modified Cu/Zn/Al/Zr catalysts via hydrotalcite-like precursors for CO₂ hydrogenation to methanol. *Catal. Commun.* **2014**, *50*, 78–82. [[CrossRef](#)]
35. Santiago, M.; Barbera, K.; Ferreira, C.; Curulla-Ferré, D.; Kolb, P.; Pérez-Ramírez, J. By-product co-feeding reveals insights into the role of zinc on methanol synthesis catalysts. *Catal. Commun.* **2012**, *21*, 63–67. [[CrossRef](#)]
36. Akbarzadeh, H.; Abbaspour, M.; Salemi, S. Carbon monoxide adsorption on the single-walled carbon nanotube supported gold-silver nanoalloys. *New J. Chem.* **2016**, *40*, 310–319. [[CrossRef](#)]
37. Yang, H.; Gao, P.; Zhang, C.; Zhong, L.; Li, X.; Wang, S.; Wang, H.; Wei, W.; Sun, Y. Core-shell structured Cu@m-SiO₂ and Cu/ZnO@m-SiO₂ catalysts for methanol synthesis from CO₂ hydrogenation. *Catal. Commun.* **2016**, *84*, 56–60. [[CrossRef](#)]
38. Kaluza, S.; Behrens, M.; Schiefenhövel, N.; Kniep, B.; Fischer, R.; Schlögl, R.; Muhler, M. A Novel Synthesis Route for Cu/ZnO/Al₂O₃ Catalysts used in Methanol Synthesis: Combining Continuous Consecutive Precipitation with Continuous Aging of the Precipitate. *ChemCatChem* **2011**, *3*, 189–199. [[CrossRef](#)]
39. Zhang, P.; Araki, Y.; Feng, X.; Li, H.; Fang, Y.; Chen, F.; Shi, L.; Peng, X.; Yoneyama, Y.; Yang, G.; et al. Urea-derived Cu/ZnO catalyst being dried by supercritical CO₂ for low-temperature methanol synthesis. *Fuel* **2020**, *268*, 117213. [[CrossRef](#)]
40. Ay, S.; Ozdemir, M.; Melikoglu, M. Effects of metal promotion on the performance, catalytic activity, selectivity and deactivation rates of Cu/ZnO/Al₂O₃ catalysts for methanol synthesis. *Chem. Eng. Res. Des.* **2021**, *175*, 146–160. [[CrossRef](#)]

41. Spath, P.L.; Dayton, D.C. Preliminary Screening—Technical and Economic Assessment of Synthesis Gas to Fuels and Chemicals with Emphasis on the Potential for Biomass-Derived Syngas. Available online: www.nrel.gov/docs/fy04osti/34929.pdf (accessed on 20 September 2022).
42. Chen, F.; Gao, W.; Wang, K.; Wang, C.; Wu, X.; Liu, N.; Guo, X.; He, Y.; Zhang, P.; Yang, G.; et al. Enhanced performance and stability of Cu/ZnO catalyst by introducing MgO for low-temperature methanol synthesis using methanol itself as a catalytic promoter. *Fuel* **2022**, *315*, 123272. [[CrossRef](#)]
43. Wernicke, H.-J.; Plass, L.; Schmidt, F. Methanol generation. In *Methanol: The Basic Chemical and Energy Feedstock of the Future*; Bertau, M., Offermanns, H., Plass, L., Schmidt, F., Wernicke, H.-J., Eds.; Springer: Berlin/Heidelberg, Germany, 2014; pp. 51–300.
44. Poto, S.; van Berkel, D.V.; Gallucci, F.; d'Angelo, M.F.N. Kinetic modeling of the methanol synthesis from CO₂ and H₂ over a CuO/CeO₂/ZrO₂ catalyst: The role of CO₂ and CO hydrogenation. *Chem. Eng. J.* **2022**, *435*, 134946. [[CrossRef](#)]
45. Li, Z.; Du, T.; Li, Y.; Jia, H.; Wang, Y.; Song, Y.; Fang, X. Water- and reduction-free preparation of oxygen vacancy rich Cu-ZnO-ZrO₂ catalysts for promoted methanol synthesis from CO₂. *Fuel* **2022**, *322*, 124264. [[CrossRef](#)]
46. Ovesen, C.V. Kinetic Modeling of Reactions on Cu Surfaces. Ph.D. Thesis, Laboratory of Applied Physics, Technical University of Denmark, Lyngby, Denmark, 1992.
47. Clausen, B.S.; Steffensen, G.; Fabius, B.; Villadsen, J.; Feidenhans'l, R.; Topsøe, H. In situ cell for combined XRD and on-line catalysis tests: Studies of Cu-based water gas shift and methanol catalysts. *J. Catal.* **1991**, *132*, 524–535. [[CrossRef](#)]
48. Fujitani, T.; Nakamura, J. The chemical modification seen in the Cu/ZnO methanol synthesis catalysts. *Appl. Catal. A Gen.* **2000**, *191*, 111–129. [[CrossRef](#)]
49. Ostrovskii, V.E. Mechanisms of methanol synthesis from hydrogen and carbon oxides at Cu–Zn-containing catalysts in the context of some fundamental problems of heterogeneous catalysis. *Catal. Today* **2002**, *77*, 141–160. [[CrossRef](#)]
50. Doluda, V.Y.; Sulman, E.M.; Matveeva, V.G.; Sulman, M.G.; Bykov, A.V.; Lakina, N.V.; Sidorov, A.I.; Valetsky, P.M.; Bronstein, L.M. Phenol Catalytic Wet Air Oxidation Over Ru Nanoparticles Formed in Hypercrosslinked Polystyrene. *Top. Catal.* **2013**, *56*, 688–695. [[CrossRef](#)]
51. Manaenkov, O.V.; Matveeva, V.G.; Sulman, E.M.; Filatova, A.E.; Makeeva, O.Y.; Kislitza, O.V.; Sidorov, A.I.; Doluda, V.Y.; Sulman, M.G. Ru-Containing Polymeric Catalysts for Cellulose Conversion to Polyols. *Top. Catal.* **2014**, *57*, 1476–1482. [[CrossRef](#)]
52. Sapunov, V.N.; Stepacheva, A.A.; Sulman, E.M.; Warna, J.; Maki-Arvela, P.; Sulman, M.G.; Sidorov, A.I.; Stein, B.D.; Murzin, D.Y.; Matveeva, V.G. Stearic acid hydrodeoxygenation over Pd nanoparticles embedded in mesoporous hypercrosslinked polystyrene. *J. Ind. Eng. Chem.* **2017**, *46*, 426–435. [[CrossRef](#)]
53. Thommes, M.; Kaneko, K.; Neimark, A.V.; Olivier, J.P.; Rodriguez-Reinoso, F.; Rouquerol, J.; Sing, K.S. Physisorption of Gases, with Special Reference to the Evaluation of Surface Area and Pore Size Distribution (IUPAC Technical Report). *Pure Appl. Chem.* **2015**, *87*, 1051–1069. [[CrossRef](#)]
54. Guo, H.-L.; Zhu, Q.; Wu, X.-L.; Jiang, Y.-F.; Xie, X.; Xu, A.-W. Oxygen deficient ZnO_{1-x} nanosheets with high visible light photocatalytic activity. *Nanoscale* **2015**, *7*, 7216–7223. [[CrossRef](#)] [[PubMed](#)]
55. Armelao, L.; Barreca, D.; Bottaro, G. ZnO:Er(III) Nanosystems Analyzed by XPS. *Surf. Sci. Spectra* **2006**, *13*, 9–16. [[CrossRef](#)]
56. Pauly, N.; Yubero, F.; Espinós, J.P.; Tougaard, S. XPS primary excitation spectra of Zn 2p, Fe 2p, and Ce 3d from ZnO, α-Fe₂O₃, and CeO₂. *Surface Interface Anal.* **2018**, *51*, 353–360. [[CrossRef](#)]
57. Arefi, M.; Rezaei-Zarchi, S. Synthesis of Zinc Oxide Nanoparticles and Their Effect on the Compressive Strength and Setting Time of Self-Compacted Concrete Paste as Cementitious Composites. *Int. J. Mol. Sci.* **2012**, *13*, 4340–4350. [[CrossRef](#)]
58. Bindu, P.; Thomas, S. Estimation of lattice strain in ZnO nanoparticles: X-ray peak profile analysis. *J. Theor. Appl. Phys.* **2014**, *8*, 123–134. [[CrossRef](#)]
59. Ovesen, C.V.; Clausen, B.S.; Schiotz, J.; Stoltze, P.; Topsøe, H.; Nørskov, J.K. Kinetic Implications of Dynamical Changes in Catalyst Morphology during Methanol Synthesis over Cu/ZnO Catalysts. *J. Catal.* **1997**, *168*, 133–142. [[CrossRef](#)]
60. Kuzmin, A.; Larcheri, S.; Rocca, F. Zn K-edge XANES in nanocrystalline ZnO. *J. Phys. Conf. Ser.* **2007**, *93*, 012045. [[CrossRef](#)]
61. Molenbroek, A.M.; Helveg, S.; Topsøe, H.; Clausen, B.S. Nano-particles in heterogeneous catalysis. *Top. Catal.* **2009**, *52*, 1303–1311. [[CrossRef](#)]
62. Ankudinov, A.L.; Ravel, B.; Rehrand, J.J.; Conradson, S.D. Real-space multiple-scattering calculation and interpretation of x-ray-absorption near-edge structure. *Phys. Rev. B* **1998**, *58*, 7565–7576. [[CrossRef](#)]
63. Frenkel, A.I.; Kleinfeld, O.; Wasserman, S.R.; Sagi, I. Phase speciation by extended x-ray absorption fine structure spectroscopy. *J. Chem. Phys.* **2002**, *116*, 9449–9456. [[CrossRef](#)]
64. Bykov, A.V.; Rubin, M.A.; Sulman, M.G.; Sulman, E.M. Liquid phase synthesis of methanol using a commercial copper-zinc catalyst. *Catal. Ind.* **2014**, *1*, 60–67.
65. Corro, G.; Cebada, S.; Pal, U.; García Fierro, J.L.; Alvarado, J. Hydrogen-reduced Cu/ZnO composite as efficient reusable catalyst for diesel particulate matter oxidation. *Appl. Catal. B Environ.* **2015**, *165*, 555–565. [[CrossRef](#)]

Disclaimer/Publisher's Note: The statements, opinions and data contained in all publications are solely those of the individual author(s) and contributor(s) and not of MDPI and/or the editor(s). MDPI and/or the editor(s) disclaim responsibility for any injury to people or property resulting from any ideas, methods, instructions or products referred to in the content.